

importance in affecting the magnitude of the ^{18}O -induced shift in ^{13}C NMR spectroscopy, at least in these symmetrically substituted examples. The primary factor affecting the magnitude of this isotope effect is the structure of the carbon-oxygen functional group.

Acknowledgment. This investigation was supported by Research Grant GM 27003-10 from the National Institute of General Medical Sciences. We thank Professor Robert Benkeser and Dr. Charles Muth for aiding us in obtaining two of the compounds used in this study.

Chemical, Spectral, Structural, and Charge Transport Properties of the "Molecular Metals" Produced by Iodination of Nickel Phthalocyanine

Charles J. Schramm, Raymond P. Scaringe, Djordje R. Stojakovic, Brian M. Hoffman,* James A. Ibers,* and Tobin J. Marks*¹

Contribution from the Department of Chemistry and the Materials Research Center, Northwestern University, Evanston, Illinois 60201. Received February 11, 1980

Abstract: This paper presents a detailed study of the solid-state chemical, spectral, structural, and charge transport properties of the materials which result from treating nickel phthalocyanine (NiPc) with elemental iodine. A range of NiPcI_x stoichiometries is obtained where $x = 0$ to ca. 3.0; electrical conductivities of compressed polycrystalline samples are comparable with those of other "molecular metals". Single crystals were obtained for $\text{NiPcI}_{1.0}$. These crystallize in the space group D_{4h}^2-P4/mcc , with two formula units in a unit cell having dimensions $a = 13.936$ (6), $c = 6.488$ (3) Å. Full-matrix least-squares refinement of 65 variables gave a final value of the conventional R index (on F) of 0.042 for 375 reflections having $F_o^2 > 3\sigma(F_o^2)$. The crystal structure consists of stacked, planar NiPc units (staggered by 39.5°) and disordered chains of iodine atoms extending in the c direction. The NiPc units have crystallographically imposed symmetry $4/m$. The interplanar Ni-Ni separation is 3.244 (2) Å, and the intramolecular Ni-N distance, 1.887 (6) Å. Analysis of the diffuse scattering pattern arising from disordered iodine chains reveals that iodine is present as I_3^- . An I-I distance of 3.00 Å and a I...I distance of 3.72 Å are derived from the diffuse scattering. Resonance Raman and iodine-129 Mössbauer spectroscopic measurements indicate that iodine is present predominantly if not exclusively as I_3^- for all NiPcI_x where $x \leq 3$. Optical spectroscopic and X-ray powder diffraction studies of the $x \neq 1.0$ phases suggest that mixtures of several discrete phases are present. Single-crystal electron spin resonance studies (ESR) of $\text{NiPcI}_{1.0}$ reveal that the iodine oxidation is ligand centered yielding π radical cations. The charge distribution thus can best be represented as $[\text{Ni}^{\text{II}}\text{Pc}]^{0.33+}(\text{I}_3^-)_{0.33}$, although there is ca. 0.002 unit of charge back-transferred from each I_3^- unit to the metallomacrocyclic stack. Susceptibility measurements by ESR and static techniques can be interpreted in terms of a narrow bandwidth metal (ca. 0.37 eV) and a significant contribution from van Vleck paramagnetism. The electrical conductivity of $\text{NiPcI}_{1.0}$ crystals has been investigated by four-probe techniques. Room-temperature conductivities along the crystallographic stacking direction are in the range 260–750 $\Omega^{-1}\text{cm}^{-1}$ and carrier mean free paths are in the range 3.3–8.2 Å. The temperature dependence of the conductivity is metallic ($\rho \sim T^{1.9\pm 0.2}$) down to ca. 55 K, at which point there occurs an abrupt reduction in conductivity. Neither the resonance Raman of the I_3^- , the ESR line width, nor the magnetic susceptibility is sensitive to this transition.

Present experience indicates that for a coordination compound to form an electrically conductive molecular crystal two criteria are highly desirable, if not essential. First, the metal-ligand molecules must be arrayed in close communication and in crystallographically similar environments. Second, the metal-ligand complex must adopt a nonintegral formal oxidation state.² The latter characteristic has been referred to as "partial oxidation", "mixed valence", or "incomplete charge transfer", and, although this state has generally been effected with oxidizing agents, in principle it could equally well be achieved by a partial reduction. The highly conductive coordination compounds studied to date, as exemplified by the tetracyanoplatinate materials, represent a class of materials in which transport properties can be understood almost completely in terms of the charge carriers being confined to a conducting spine of metal atoms.² The coordinated ligands (e.g., CN^-) are essential in dictating the structural and electronic properties of the metal-atom chain, but appear to play little or no direct role in the charge-transport process.

Mixed-valent coordination complexes of an entirely different variety are represented by a growing number of partially oxidized materials containing metal complexes of planar, conjugated organic ligands.³⁻⁵ Especially in the case of iodine oxidants, it is possible to synthesize broad classes of nonintegral oxidation state materials,

(3) (a) Petersen, J. L.; Schramm, C. S.; Stojakovic, D. R.; Hoffman, B. M.; Marks, T. J. *J. Am. Chem. Soc.* **1977**, *99*, 286–288. (b) Schramm, C. S.; Stojakovic, D. R.; Hoffman, B. M.; Marks, T. J. *Science* **1978**, *200*, 47–48.

(4) (a) Phillips, T. E.; Hoffman, B. M. *J. Am. Chem. Soc.* **1977**, *99*, 7734–7736. (b) Hoffman, B. M.; Phillips, T. E.; Schramm, C. J.; Wright, S. K. In "Molecular Metals", Hatfield, W. E., Ed.; Plenum Press: New York, 1979; pp 393–398. (c) Wright, S. K.; Schramm, C. J.; Phillips, T. E.; Scholler, D. M.; Hoffman, B. M. *Synth. Met.* **1979**, *80*, 1, 43–51. (d) Phillips, T. E.; Scaringe, R. P.; Hoffman, B. M.; Ibers, J. A. *J. Am. Chem. Soc.* **1980**, *102*, 3435–3444.

(5) (a) Marks, T. J. In ref 2a, pp 594–616. (b) Cowie, M.; Gleizes, A.; Grynkeiwich, G. W.; Kalina, D. W.; McClure, M. S.; Scaringe, R. P.; Teitelbaum, R. C.; Ruby, S. L.; Ibers, J. A.; Kannewurf, C. R.; Marks, T. J. *J. Am. Chem. Soc.* **1979**, *101*, 2921–2936. (c) Brown, L. D.; Kalina, D. W.; McClure, M. S.; Ruby, S. L.; Schultz, S.; Ibers, J. A.; Kannewurf, C. R.; Marks, T. J. *ibid.* **1979**, *101*, 2937–2947. (d) Kalina, D. W.; Lyding, J. W.; McClure, M. S.; Kannewurf, C. R.; Marks, T. J. *J. Am. Chem. Soc.*, in press. (e) Lin, L.-S.; Marks, T. J.; Kannewurf, C. R.; Lyding, J. W.; McClure, M. S.; Ratajack, M. T.; Whang, T.-C. *J. Chem. Soc., Chem. Commun.*, in press. (f) Schoch, K. F., Jr.; Kundalkar, B. R.; Marks, T. J. *J. Am. Chem. Soc.* **1979**, *101*, 7071–7073. (g) Marks, T. J.; Schoch, K. F., Jr.; Kundalkar, B. R. *Synth. Met.* **1980**, *1*, 337–347.

(1) Camille and Henry Dreyfus Teacher-Scholar.

(2) (a) Miller, J. S.; Epstein, A. J., Eds. *Ann. N.Y. Acad. Sci.* **1978**, *313*. (b) Keller, H. J., Ed. "Chemistry and Physics of One Dimensional Metals", Plenum Press: New York, 1977. (c) Miller, J. S.; Epstein, A. J. *Prog. Inorg. Chem.* **1976**, *20*, 1–151. (d) Keller, H. J., Ed. "Low Dimensional Cooperative Phenomena", Plenum Press: New York, 1975.

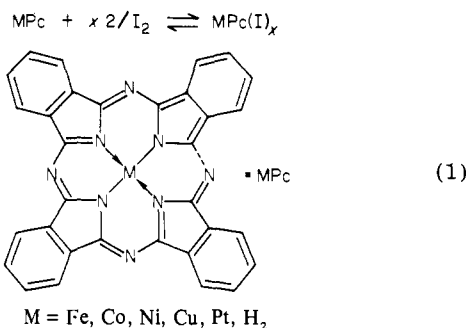
Table I. Reaction Conditions^a and Analytical Data for NiPcI_x Samples

x	wt (mmol) NiPc, g	wt (mmol) I ₂ , g	vol solvent, ^a mL	elemental anal., calcd (found)			
				C	H	N	I
0.30	0.71 (1.24)	b	50	63.07 (63.89)	2.63 (2.58)	18.40 (19.16)	6.26 (6.37)
0.58	0.30 (0.53)	0.056 (0.22)	5	59.83 (58.68)	2.49 (2.40)	17.43 (17.71)	11.08 (11.06)
1.07	0.30 (0.53)	0.11 (0.43)	5	54.34 (54.77)	2.26 (2.20)	15.85 (15.58)	
1.44	0.30 (0.53)	0.16 (0.63)	5	50.96 (51.00)	2.12 (2.49)	14.86 (14.69)	
2.79	0.56 (0.92)	b	100	41.51 (42.48)	1.73 (1.79)	12.11 (12.51)	38.30 (39.36)
3.81	0.34 (0.60)	b	100	36.41 (36.60)	1.52 (1.75)	10.62 (10.45)	

^a See Experimental Section for procedures. ^b A saturated solution of iodine in chlorobenzene was employed.

and furthermore, using resonance Raman,⁵ iodine Mössbauer,⁵ as well as diffuse X-ray scattering techniques,⁶ to identify the form of iodine present (I₂, I⁻, I₃⁻, I₅⁻, or mixtures thereof), hence the degree of incomplete charge transfer. Among the known classes of partially oxidized metallomacrocycles, the metallophthalocyanines (MPc)³ stand out in terms of charge-transport properties, chemical flexibility, and technological accessibility.

We have previously shown that iodine oxidation of a variety of metallophthalocyanines (as well as the metal-free derivatives) produces an extensive new class of highly conductive (as judged by measurements on compressed polycrystalline samples) molecular materials with a wide range of dopant stoichiometries (eq 1).^{3a} Subsequently we reported preliminary single crystal studies



on NiPcI_{1.0}, which demonstrate that it is a "molecular metal" down to 55 K and that carrier mean free paths compare favorably with those of the most conductive stacked molecular materials known.^{3b} In the present study, we focus in depth on the properties of the NiPcI_{1.0} and NiPcI_x materials. This includes X-ray diffraction, optical, resonance Raman, iodine Mössbauer, electron spin resonance, magnetic susceptibility, and charge transport measurements. It is seen that the iodinated nickel phthalocyanines are indeed "molecular metals". In the case of NiPcI_{1.0} single crystals, the crystal structure has been precisely characterized as stacks of NiPc^{0.33+} units and parallel chains of I₃⁻ counterions with a disorder among these latter chains. The electrical conductivity in the stacking direction is metallic down to 55 K, and this interpretation is supported by essentially constant magnetic susceptibility. At ca. 55 K, NiPcI_{1.0} undergoes a metal-semiconductor transition; this transition does not manifest itself in the resonance Raman spectrum, nor, surprisingly, in the magnetic susceptibility or ESR line width.

In subsequent phthalocyanine contributions we will explore the effects of metal ion and ligand modification upon the electronic and structural properties.

Experimental Section

Nickel phthalocyanine was purchased from Eastman Kodak Co. and sublimed at 400 °C (10⁻³ Torr) before use. Solvents were of analytical reagent or spectrograde quality. Elemental analyses were performed by Micro-Tech Laboratories, Inc., Skokie, Ill., or Miss H. Beck, Northwestern Analytical Services Laboratory.

Synthesis of NiPcI_x Materials. To prepare polycrystalline samples of various stoichiometries, finely powdered nickel phthalocyanine was stirred

in a closed vial with various amounts of iodine in chlorobenzene for 48 h. Longer reaction times produced no detectable changes in spectral or transport properties. The iodinated nickel phthalocyanine was collected by centrifugation, washed with several portions of hexane, and dried under a stream of dry nitrogen. Relevant synthetic information and analytical data are compiled in Table I. Single crystals of NiPcI_{1.0} were grown in an H-tube by diffusing together solutions of iodine and NiPc in either 1,2,4-trichlorobenzene or 1-chloronaphthalene.

Anal. Calcd for C₃₂H₁₆I_{1.0}N₈Ni: C, 55.02; H, 2.31; N, 16.04; I, 18.17. Found: C, 54.61; H, 2.34; N, 16.09; I, 18.37.

X-ray Diffraction Study of NiPcI_{1.0}. Single crystals of this material were grown as described above. On the basis of a series of Weissenberg and precession photographs the crystals were assigned to Laue group 4/*mmm* of the tetragonal system. The only systematic absences observed were for *0kl* and *hhl* with *l* odd; hence the space group is either *P4/mcc* or *P4cc*. Excellent agreement among Friedel pairs and successful refinement of the structure support the choice of space group *D_{4h}²-P4/mcc*. The cell constants of *a* = 13.936 (6), *c* = 6.488 (3) Å were obtained by usual procedures⁷ using the setting angles on a FACS-I diffractometer of 15 hand-centered reflections having 2θ (Cu Kα₁) ≥ 30°. The observed density of 1.78 (4) g/cm³, obtained by flotation of the crystals in ZnBr₂ solutions, may be compared with that of 1.84 g/cm³ calculated for two formula units in the cell.

Although most crystals examined exhibited Bragg peaks with considerable structure, the small specimen selected for data collection displayed only slight splittings. Data were collected at room temperature using Cu Kα radiation prefiltered with 1-mil Ni foil by methods standard in this laboratory.⁷ Crystal data and details of collection of Bragg peak intensity data are summarized in Table II.

Laue and oscillation photography displayed the presence of diffuse scattering in addition to normal Bragg scattering. Diffuse scattering was confined to planes perpendicular to the *c** axis with a spacing (*c**) between such planes being 2*c**/3. Except for superstructure reflections the intensity within each plane falls off smoothly with increasing scattering angle, but it changes markedly from one layer to the next. In particular, no diffuse layers with *l*' = 3*n* were observed.

The relative intensities of the diffuse layers were obtained by X-ray counter techniques employing Cu Kα radiation and a graphite monochromator. The sample area was enclosed in a polyethylene bag filled by a constant flow of helium to reduce atmospheric scattering. The crystal used was not the one employed for collection of Bragg peaks but rather was a needle of octagonal cross section approximately 0.8 mm long and with separations of 0.06 mm between opposite axial faces. Reciprocal space was sampled point by point along a line perpendicular to the diffuse planes. Since no diffuse layers with *l*' = 3*n* were observed photographically, intensity data were not gathered for these layers. Data were collected out to the limit of the Cu sphere, which corresponds to *l*' = 11. Counting times for each point ranged from 600 to 2000 s. Peak and background points were separated by examining plots of the data. Intensities were corrected for polarization, geometrical factors, and absorption.^{8,9}

Solution and Refinement of the Structure. An origin-removed sharpened Patterson function indicated that all iodine atoms were at relative

(7) Corfield, P. W. R.; Doedens, R. J.; Ibers, J. A. *Inorg. Chem.* **1967**, *6*, 197-204.

(8) The Northwestern absorption program, AGNOST, includes both the Coppens-Leiserowitz-Rabinovich logic for Gaussian integration and the Tompa analytical method. In addition to various local programs for the CDC-600 computer, modified versions of the following programs were employed: Zalkin's FORDAP Fourier summation program, Johnson's ORTEP thermal ellipsoid plotting program, and Busing's and Levy's ORFFE error function program. Our full-matrix, least-squares program, NUCLS, in its nongroup form closely resembles the Busing-Levy ORFLS program. The diffractometer was run under the disk-oriented Vanderbilt system (Lenhart, P. G. *J. Appl. Crystallogr.* **1975**, *8*, 568-570).

(9) Azaroff, L. V. *Acta Crystallogr.* **1955**, *8*, 701-704.

(6) (a) Scaringe, R. P.; Ibers, J. A. *Acta Crystallogr. Sect. A* **1979**, *35*, 803-810. (b) Megtert, S.; Pouget, J. P.; Comès, R. In ref 2a, pp 234-243. (c) Endres, H.; Keller, H. J.; Mëgnamisi-Belombë, M.; Moroni, W.; Pritzkow, H.; Weiss, J.; Comès, R. *Acta Crystallogr., Sect. A* **1976**, *32*, 945-957.

Table II. Crystal Data and Experimental Details

compd	Ni(phthalocyanine)I
formula	NiC ₃₂ H ₁₆ N ₈ I
formula wt	698.15 amu
cell: <i>a</i>	13.936(6) Å
<i>c</i>	6.488(3) Å
<i>V</i>	1260.1 Å ³
<i>Z</i>	2
density: calcd	1.84 g/cm ³
obsd	1.78(4) g/cm ³
space group	<i>D</i> _{4h} ² - <i>P4/mcc</i>
crystal shape	needle of octagonal cross section bounded by faces of the forms {100}, {110}, and {001} with separations of 0.040, 0.042, and 0.712 mm, respectively
radiation	Cu Kα ₁
linear abs. coefficient	111.4 cm ⁻¹
transmission coefficients	0.499–0.713
take-off angle	3.5°
receiving aperture	5.8 mm high × 5.0 mm wide
	26 cm from crystal
receiving counter	34 cm from crystal
scan speed	2°/min
scan width	0.85° below Kα ₁ to 0.9° above Kα ₂ , for 2.0 ≤ 2θ ≤ 90.0°
	1.0 below Kα ₁ to 1.0 above Kα ₂ , for 90.0 ≤ 2θ ≤ 125.0°
	1.5 below Kα ₁ to 1.0 above Kα ₂ , for 125.0 ≤ 2θ ≤ 160.0°
background counts	40 s total for singly scanned peaks
data collected	<i>h</i> ≥ <i>k</i> ≥ 0 ± 1 2θ < 90°
	<i>h</i> ≥ <i>k</i> ≥ 0 + 1 90° < 2θ < 160°
unique data (after averaging Friedel pairs)	630
unique data with <i>F</i> ₀ ² > 3σ(<i>F</i> ₀ ²)	375
<i>R</i> for last cycle of refinement	0.042
<i>R</i> _w on <i>F</i> ₀ ²	0.051
<i>R</i> final cycle of <i>F</i> ₀ ²	0.058 (<i>F</i> ₀ ² > 3σ(<i>F</i> ₀ ²))
<i>R</i> _w	0.113
final no. of variables	65

positions ±1/2, ±1/2, ±1/4 from the nickel atoms. Many of the iodine to ring atom vectors were evident at *w* = 1/4, leading to the correct orientation of the ring and the relative positions of most of the light atoms. The orientation of the chelate ring with respect to the crystallographic axes precluded the possibility of site symmetry 422 for the nickel atom. With the added constraint *Z* = 2, site symmetry 4/*m* was the only remaining possibility in *P4/mcc*. Initial refinements were carried out on *F*₀², using the 375 unique reflections having *F*₀² > 3σ(*F*₀²). After idealizing the ring atom positions obtained from the vector map, one cycle of least-squares refinement with variable isotropic thermal parameters resulted in values of 0.125 and 0.161, respectively, for *R* and *R*_w, the usual agreement indices. Two cycles of refinement with variable anisotropic thermal parameters for all nonhydrogen atoms reduced those values to 0.058 and 0.074, respectively. The subsequent difference Fourier map indicated the positions of all hydrogen atoms and also one small peak (~1.0 e Å⁻³) located about 1 Å from the iodine position along the *z* axis. All hydrogen atoms were found to be close to their idealized position (C–H = 0.95 Å); these positions were used and not varied in the least-squares process for the remainder of the refinement. Each hydrogen atom was assigned a fixed isotropic thermal parameter equal to 1 Å² greater than that of the carbon atom to which it is bonded. In the final cycle of refinement on |*F*₀|, there were 375 observations and 65 variables and the resultant values of *R* and *R*_w were 0.043 and 0.051, respectively. No positional parameters exhibited a significant shift during this cycle.

Two additional cycles of refinement of *F*₀² (including *F*₀² < 0) increased the number of available observations to 630 and resulted in the expected decrease in the estimated standard deviations of all variables. In this first cycle of refinement the occupancy factor of the iodine was also allowed to vary yielding a value of 0.995 (6) iodine atoms per site; in the final cycle the occupancy was fixed at one iodine per site. The final cycle of least-squares refinement then involved full-matrix refinement of 65 variables with 630 observations; the final values of *R* and *R*_w (on *F*₀²) are 0.057 and 0.113, respectively. The *R* index on *F*₀ for those reflections having *F*₀² > 3σ(*F*₀²) is 0.042. With the exception of one small peak (0.7 e Å⁻³) at the Ni position and several small peaks (0.5–0.6 e Å⁻³) along

the iodine chain the final difference Fourier synthesis is featureless. The final positional and thermal parameters are given in Table III, and root-mean-square amplitudes of vibration in Table IV.¹⁰ A listing of structure amplitudes is available.¹⁰ A minus sign preceding |*F*₀| indicates a negative value for *F*₀².

Resonance Raman Measurements. Spectra were recorded on a 0.85-m Spex 1401 double monochromator spectrometer using 5145-Å Ar⁺ excitation. Samples were studied in spinning (1800 rpm) 5- or 12-mm Pyrex tubes using a 180° backscattering illumination geometry. A number of scans were made of each sample (the first at lowest possible laser power) to check for possible sample decomposition. Spectra were calibrated with the exciting line (*ν*₀) or laser plasma lines. Low-temperature studies were performed with the apparatus described previously.^{5b,11}

Electronic Spectroscopy. Optical spectra were recorded on a Cary 17D spectrophotometer. Solid samples were examined as Nujol mulls between quartz plates. Several scans were made of each sample to check for possible decomposition.

X-ray Powder Diffraction Measurements. Samples were studied using a Philips Electronic Instruments Model XRG-5000 powder diffractometer with a pyrolytic graphite monochromator in the diffracted beam geometry and Cu Kα radiation. Samples were examined as 4.5 × 39 mm pressed pellets. Data were collected at a scan rate of 0.25°/min and recorded on a strip-chart recorder.

Iodine-129 Mössbauer Spectroscopy. The sample was prepared by the reaction of NiPc in chlorobenzene with ¹²⁹I₂ prepared as described previously. Elemental analysis showed it to be of stoichiometry NiPcI_{1.16}. The Mössbauer spectrometer was that described elsewhere (⁶⁶Zn/¹²⁹Te source, standard transmission geometry, ⁵⁷Fe calibrated velocity generated by a feedback-controlled vibrator with sinusoidal acceleration^{5b,11}). The absorber was prepared by thoroughly powdering the NiPcI_{1.16} material and diluting it with boron nitride. Both source and absorber were maintained at 4.2 K during data acquisition. Data were collected with a proportional counter and 400-channel multichannel analyzer operating in the time mode. Data processing utilized the program GENFIT,^{12a} which finds the optimum isomer shifts, quadrupole coupling constants, line widths, site populations, and asymmetry parameters via nonlinear least-squares minimization of the difference between the calculated and observed spectrum. The goodness of fit is judged by the previously defined parameter "Misfit".^{12,13}

Electron Spin Resonance Studies. Measurements were carried out using a highly modified Varian E-4 X-band ESR spectrometer, with 100-kHz field modulation. Temperatures in the range 300–90 K were obtained by regulation of the flow rate of cooled liquid nitrogen boiloff gas. A calibrated copper–constantan thermocouple placed within 1.0 cm of the sample monitored the temperature to within ±1 K. The extended temperature range 300–15 K was obtained with an Air Products LTD-3 cryostat system using liquid helium. The temperature, stable to better than ±1 K, was monitored by a calibrated rhodium–gold thermocouple placed in the immediate vicinity of the sample.

For the *g*-tensor measurements, 2,2-phenyl-1-picrylhydrazyl (DPPH, *g* = 2.0036) was used to provide absolute field calibration. The cavity resonance frequency was measured to an accuracy of 5 ppm by a transfer oscillator technique.

The sample crystals of NiPcI_{1.0} were mounted on a Teflon crystal holder with silicone grease and then the holder was pressed into a piece of quartz tubing. This was attached to a rotating goniometer head of standard design mounted firmly to the resonance cavity. Rotation angles could be measured to a precision of ±1.0°.

The integrated ESR intensity was obtained by electronically integrating the first derivative signal and then measuring the area under the absorption curve. For these approximately Lorentzian signals, scans of 20 times the line width were run; this limits the error caused by truncation to less than 5%.¹⁴ The relative ESR intensities were obtained for temperature-dependent studies and were scaled to the appropriate absolute value of the room-temperature spin susceptibility, *χ*².

DPPH, Aldrich 99% reagent grade, was used as the standard for determination of absolute spin concentration on the assumption that it

(10) See paragraph at end of paper regarding supplementary material.

(11) (a) Teitelbaum, R. C.; Ruby, S. L.; Marks, T. J. *J. Am. Chem. Soc.* **1979**, *101*, 7568–7573. (b) Teitelbaum, R. C.; Ruby, S. L.; Marks, T. J. *Ibid.*, **1980**, *102*, 3322–3328.

(12) (a) Ruby, S. L. *Moessbauer Eff. Methodol.* **1973**, *8*, 263–276. (b) The traditional goodness-of-fit parameter $\chi^2 = \sum_i [(x_i - \chi_{i,c})/\Delta x_i]^2$ gives satisfactorily small values for either a good metal (the calculated values $\chi_{i,c}$ agree well with the data x_i , or for a poor experiment (Δx_i is large).

(13) Shenoy, G. K.; Friedt, J. M.; Maletta, H.; Ruby, S. L. *Moessbauer Eff. Methodol.* **1974**, *9*, 277–305.

(14) Wertz, J. E.; Bolton, J. R. "Electron Spin Resonance"; McGraw-Hill: New York, 1972.

Table III. Positional and Thermal Parameters for the Atoms of NiPcI

ATOM	A			B					
	x	y	z	B11	B22	B33	B12	B13	B23
I	1/2	1/2	1/4	6.0215)	6.02	56.08(52)	0	1	0
N Γ	0	0	0	3.84(8)	3.84	14.32(52)	0	1	0
N(1)	0.12241(40)	0.05780(39)	0	4.43(36)	3.13(31)	14.3(14)	0.20(28)	1	0
N(2)	0.08299(42)	0.22679(43)	0	4.25(39)	4.56(33)	16.1(15)	-0.10(32)	1	0
C(1)	0.14278(51)	0.15335(47)	0	4.50(47)	3.00(41)	11.5(14)	-0.43(30)	1	0
C(2)	0.24543(51)	0.17133(51)	0	3.79(40)	5.04(46)	16.1(17)	-0.66(35)	1	0
C(3)	0.30056(58)	0.25379(56)	0	6.17(50)	4.67(47)	21.8(20)	-0.22(40)	1	0
C(4)	0.40001(62)	0.24464(63)	0	5.25(51)	6.01(56)	34.0(28)	-1.66(45)	1	0
C(5)	0.44165(60)	0.15366(66)	0	4.29(48)	6.94(61)	36.0(28)	-1.17(44)	1	0
C(6)	0.38723(54)	0.07071(59)	0	4.73(49)	5.12(50)	28.0(23)	0.02(38)	1	0
C(7)	0.28786(52)	0.08089(55)	0	3.90(42)	5.53(52)	15.5(18)	0.15(36)	1	0
C(8)	0.21005(45)	0.01064(61)	0	3.50(35)	5.37(50)	12.0(15)	-0.57(37)	1	0
H1 C(3)	0.271	0.318	0	4.8					
H1 C(4)	0.440	0.301	0	5.9					
H1 C(5)	0.512	0.150	0	5.6					
H1 C(6)	0.417	0.007	0	4.8					

^A ESTIMATED STANDARD DEVIATIONS IN THE LEAST SIGNIFICANT FIGURE(S) ARE GIVEN IN PARENTHESES IN THIS AND ALL SUBSEQUENT TABLES. ^B THE FORM OF THE ANISOTROPIC THERMAL EXPANSION IS $\exp[-(B_{11}h^2 + B_{22}k^2 + B_{33}l^2 + 2B_{12}hk + 2B_{13}hl + 2B_{23}kl)]$. THE QUANTITIES GIVEN IN THE TABLE ARE THE THERMAL COEFFICIENTS $\times 10^{-5}$.

exhibited a signal resulting from one spin per molecule. The DPPH employed had a melting point of 136–138 °C and is thus DPPH(II), which has a susceptibility corresponding to 0.95 (2) spins per molecule.¹⁵ The DPPH was dispersed in potassium bromide for ease of handling and to achieve a spin concentration per sample size more characteristic of those found in the iodine-oxidized nickel phthalocyanines. Samples were packed in short quartz capillaries to a length of approximately 0.5 cm. Weights of samples were measured to an accuracy of 0.05 mg. The short tube was placed into a larger quartz tube and then into the resonance cavity. The small sample was centered in the cavity. Small sample size and careful positioning ensured that the instrument response was a function of the entire sample for each sample measured.

Static Magnetic Susceptibility Studies. These measurements were performed by the Faraday method using HgCo(SCN)₄ as a calibrant. Susceptibility studies over the temperature range 77–300 K were obtained by cooling the sample-containing Dewar vessel to liquid-nitrogen temperature (77 K) and allowing it to warm slowly to room temperature. As before, temperatures were measured to an accuracy of ± 1 K using a calibrated copper-constantan thermocouple.

Conductivity Studies on Polycrystalline Samples. Electrical conductivity data on polycrystalline NiPcI_x samples were acquired with a four-probe van der Pauw apparatus.¹⁶ Samples were prepared by pressing powders under 3-kbar pressure into cylindrical pellets, 12 mm in diameter and ca. 1 mm thick.

Single Crystal Electrical Conductivity Studies. Electrical contact to crystals mounted for four-probe measurements was made with a palladium paint prepared locally. The crystals were mounted in integrated circuit cans prepared as described elsewhere.¹⁷ Most crystals were mounted using 0.001-in. diameter aluminum wire but in some cases 0.0005-in. nickel wire was used. The coefficient of thermal expansion of Ni is half that of Al, and thus the smaller wire should place less strain on a crystal. A four-probe low-frequency ac technique, described previously, was employed for measuring the sample resistance, and the temperature was measured using a copper-constantan thermocouple located within a few millimeters of the sample.¹⁷ Temperatures in the range 85–295 K were obtained with cold N₂ gas; the extended range 20–295 K was achieved with cold helium gas obtained from liquid-helium boiloff.

The conductivity along the stacking direction of a crystal ($\sigma_{||}$) is defined in terms of a measured resistance ($R_{||}$), crystal cross-sectional area (A), and distance between voltage probes (L): $\sigma_{||} = L/(R_{||}A)$. Dimensions of crystals mounted for conductivity studies were obtained with a Gaertner toolmakers microscope whose stage movement in the x - y plane is calibrated to ± 0.002 mm. On the average, crystals were 0.02 mm in the maximum cross-sectional dimension (ω) and 2.0 mm in length; L was typically 0.7 mm. The crystals assume a variety of cross-sectional shapes and their small size precludes an accurate determination of A for a

mounted crystal. The value $\bar{A} = \omega^2$ necessarily gives an overestimate of A and the two values have been judged to have the relationship $A \approx (0.85 \pm 0.15)\bar{A}$. There is an additional uncertainty in A , because of the error in ω from the microscopic measurement itself, which is estimated to be $\Delta\omega/\omega \sim \pm 0.1$. The intercontact length (L) can be measured with more accuracy: $\Delta L/L \sim 0.03$. Thus we estimate an overall uncertainty in the cross-sectional area of $\Delta A/A \sim \pm 0.4$. The compounded uncertainties in the crystal dimensions and crystal habit lead to an estimated uncertainty in the absolute conductivity of $\Delta\sigma/\sigma \sim \pm 0.4$. Relative conductivities for a particular crystal at different temperatures are, of course, accurate to the resistance measurement ($\pm 1\%$).

Results

In this section we begin with a discussion of the chemistry and the general properties of NiPcI_x materials as regards mixed valency and transport properties. We then focus in depth on the structural, conductivity, and magnetic properties of NiPcI_{1.0} single crystals. Lastly, using the single-crystal information as a foundation, we discuss the probable nature of the NiPcI_x materials, $x \neq 1$.

NiPc Iodination Chemistry. Nickel phthalocyanine reacts with iodine solutions or vapor according to eq 1 to produce black, polycrystalline solids, NiPcI_x, for a wide range of x values (Table I). The iodination reaction is reversible and iodine can be completely removed by heating the materials in vacuo. It has also been proven possible to grow single crystals of the NiPcI_x compound where $x = 1.0$ by diffusing together solutions of NiPc and iodine. Crystals of iodinated nickel phthalocyanines could not be produced by exposing NiPc single crystals (grown by sublimation) to iodine solutions or vapor; the formation of a NiPcI_x material was accompanied by visible deterioration and crumbling of the NiPc crystals.

NiPcI_x Resonance Raman Spectroscopy. Figure 1 presents representative solid state resonance Raman spectra in the polyiodide scattering region of two of the NiPcI_x materials. The spectra of the samples with $0 < x < \text{ca. } 3.0$ are identical and exhibit the intense totally symmetric stretching fundamental of I₃⁻ at 107 cm⁻¹ along with the characteristic overtone progression.^{5,11,18} There is no evidence of I₅⁻ ($\nu \approx 160$ cm⁻¹), of I₂ coordinated to donors such as I₃⁻ ($\nu \approx 180$ cm⁻¹), or of free I₂ ($\nu \approx 200$ cm⁻¹).^{5,11,18} Strong scattering from I₃⁻ is observed when only traces of iodine are present. There was no change in the type of polyiodide as evidenced by the scattering pattern of NiPcI_{1.0} crystals when samples were cooled to 8 K or heated to 455 K. At very high iodine levels ($x \gtrsim 3.0$) scattering at 180 cm⁻¹, characteristic of I₂ coordinated to a Lewis base such as I₃⁻, is observed

(15) Duffy, Jr., W.; Strandburg, D. L. *J. Chem. Phys.* **1967**, *46*, 456.

(16) (a) Seeger, K. "Semiconductor Physics"; Springer-Verlag: New York, 1973; pp 483–487. (b) Cahen, D.; Anderson, J. R. *Rev. Sci. Instrum.* **1973**, *44*, 1567–1568.

(17) Phillips, T. E.; Anderson, J. R.; Schramm, C. J.; Hoffman, B. M. *Rev. Sci. Instrum.* **1979**, *50*, 263–265.

(18) (a) Teitelbaum, R. C.; Ruby, S. L.; Marks, T. J. *J. Am. Chem. Soc.* **1978**, *100*, 3215–3217. (b) Marks, T. J.; Webster, D. F.; Ruby, S. L.; Schultz, S. J. *Chem. Soc., Chem. Commun.* **1976**, 444–445. (c) Kalina, D. W.; Stojakovic, D. R.; Teitelbaum, R. C.; Marks, T. J., manuscript in preparation.

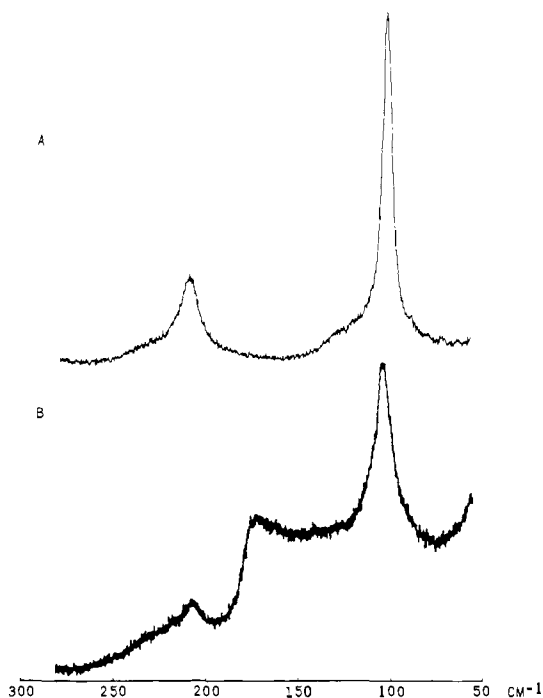


Figure 1. Resonance Raman spectra ($\nu_0 = 5145 \text{ \AA}$) of solid samples of (A) $\text{NiPcI}_{1.0}$; (B) $\text{NiPcI}_{3.81}$.

Table V. Resonance Raman Vibrational Data^a for NiPcI_x Compounds^b

x	$\nu_{I_3^-}$, cm^{-1}	other, cm^{-1}	range recorded, cm^{-1}
0.00		592 s, 687 s, 1140 m, 1340 s, 1554 vs, 1607 m	60–2000
0.30	107 s, 214 m, 322 m, 429 w	172 w	60–500
0.58	107 vs, 214 m		60–250
1.00 ^c	107 vs, 214 s, 372 m, 429 m	92 vw, 121 w	60–500
1.44	107 s, 214 m		60–250
1.56	107 s, 214 m, 322 w, 429 vw	172 vw	60–500
1.68	107 vs, 214 s, 322 m, 429 w, 535 vw	172 w, 587 w, 685 w, 1136 w, 1340 vw, 1550 w, 1606 m, 1858 m	50–2000
2.79	107 vs, 215 s, 320 m, 426 w	172 m	30–500
3.81	107 s, 215 m, 320 w	179 m, 291 vw	60–350

^a $\nu_0 = 5145 \text{ \AA}$. ^b s = strong; m = medium; w = weak; sh = shoulder; v = very. ^c Crystals over the temperature range 8–455 K.

in the NiPcI_x materials (Figure 1). Raman data are compiled in Table V.

The Raman spectrum of NiPc exhibits no scattering in the low-frequency region ($<500 \text{ cm}^{-1}$). However, transitions are observed at 592 s, 687 s, 1140 m, 1340 s, 1554 vs, and 1607 m cm^{-1} . These transitions are analogous to those observed in metalloporphyrins¹⁹ and related tetraazaannulenes;^{20,21} they can be

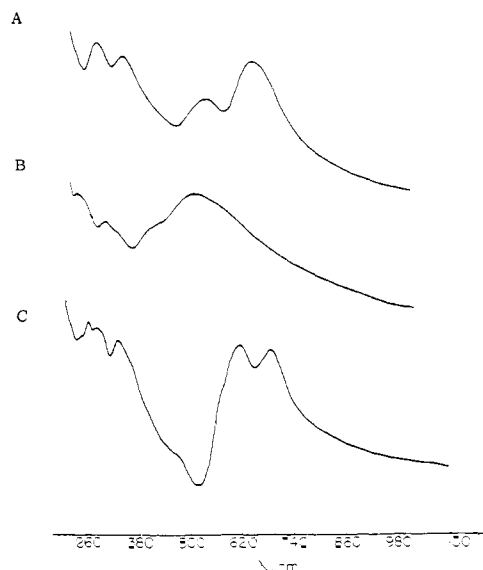


Figure 2. Electronic absorption spectra (Nujol mulls) of solid samples of (A) $\text{NiPcI}_{1.0}$; (B) $(\text{benzamide})_2\text{H}^+\text{I}_3^-$; (C) NiPc.

Table VI. Iodine-129 Mössbauer Parameters for $\text{NiPc}^{129}\text{I}_{2.16}$ ^a

parameter	site 1	site 2
δ , mm/s^b	1.34 (5)	0.27 (5)
e^2qQ , MHz^c	-1667 (10)	-862 (10)
rel population	1.0	1.7 (2)
Misfit ^d	3.4%	

^a At 4 K. ^b Vs. ZnTe. ^c For ^{129}I . ^d Defined in Experimental Section.

assigned to phthalocyanine skeletal modes, probably involving little Ni–N or C–H motion. After partial oxidation of NiPc with iodine, these skeletal modes are still observable, although qualitatively weaker and slightly displaced in energy (587 w, 685 w, 1136 w, 1340 vw, 1550 w, 1606 m cm^{-1}); in addition, a new band is observed at 1858 cm^{-1} . Analogous, oxidation-state-sensitive metal–ligand “marker” scattering is well known for metalloporphyrins¹⁹ and has been observed in the Raman spectra of partially oxidized metal glyoximates^{5b} and tetraazaannulenes.²¹

NiPcI_x Optical Spectra. In Figure 2 are shown the solid-state optical spectra of NiPc, $\text{NiPcI}_{1.0}$, and the compound $(\text{benzamide})_2\text{H}^+\text{I}_3^-$, which contains linear chains of I_3^- ions²² as does $\text{NiPcI}_{1.0}$ (vide infra). The strong absorptions at 693 and 621 nm in NiPc can be assigned to a ligand-centered $\pi-\pi^*$ transition ($a_{1u} \rightarrow e_g$ under D_{4h} symmetry);²³ the multiplicity of the band (a narrow 0–0 and weaker 0–1 transition are seen in solution) has been observed previously and has been attributed to removal of the degeneracy of the e_g level because of lowered symmetry of the crystalline environment.²⁴ Upon iodination (and change in site symmetry to C_{4h}) the $\pi-\pi^*$ transition appears as a singlet at 640 nm. In addition, a new absorption is observed at 530 nm which, on the basis of the strong $(\text{benzamide})_2\text{H}^+\text{I}_3^-$ band at 510 nm and results on other polyiodides,^{18c} is attributed to the triiodide component. It is no doubt that the transition is responsible for the resonance-enhanced I_3^- Raman scattering. Optical spectra of NiPcI_x were also studied as a function of iodine content. For $x < 1$ a shoulder on the 640-nm peak at 693 nm was detected which appears to arise from unoxidized NiPc; this observation will be discussed further in connection with the X-ray powder

(19) (a) Warshel, A. *Annu. Rev. Biophys. Bioeng.* **1977**, *6*, 273–300, and references cited therein. (b) Spiro, T. J. In “Chemical and Biochemical Applications of Lasers”, Moore, C. B., Ed.; Academic Press: New York, 1974; Vol. 1, pp 29–70, and references cited therein.

(20) (a) Woodruff, W. H.; Pastor, R. W.; Dabrowiak, J. C. *J. Am. Chem. Soc.* **1976**, *98*, 7999–8006. (b) Nafie, L. A.; Pastor, R. W.; Dabrowiak, J. C.; Woodruff, W. H. *J. Am. Chem. Soc.* **1976**, *98*, 8007–8014. (c) Clark, R. J. H.; Turtle, P. C.; Strommen, D. P.; Streusand, B.; Kincaid, J.; Nakamoto, K. *Inorg. Chem.* **1977**, *16*, 84–89. (d) Streusand, B.; Kowal, A. T.; Strommen, D. P.; Nakamoto, K. *J. Inorg. Nucl. Chem.* **1977**, *39*, 1767–1771.

(21) Lin, L.-S.; Whang, T.-C.; McClure, M. S.; Kannewurf, C. R.; Marks, T. J., submitted for publication.

(22) Reddy, J. M.; Knox, K.; Robin, M. B. *J. Chem. Phys.* **1964**, *40*, 1082–1089.

(23) (a) Marks, T. J.; Stojakovic, D. R. *J. Am. Chem. Soc.* **1978**, *100*, 1695–1705, and references cited therein. (b) Schaffer, A. M.; Gouterman, M.; Davidson, E. R. *Theor. Chim. Acta* **1973**, *30*, 9–30. (c) Edwards, L.; Gouterman, M. *J. Mol. Spectrosc.* **1970**, *33*, 292–310.

(24) Day, P.; Scregg, G.; Williams, R. J. P. *J. Chem. Phys.* **1963**, *38*, 2778–2779.

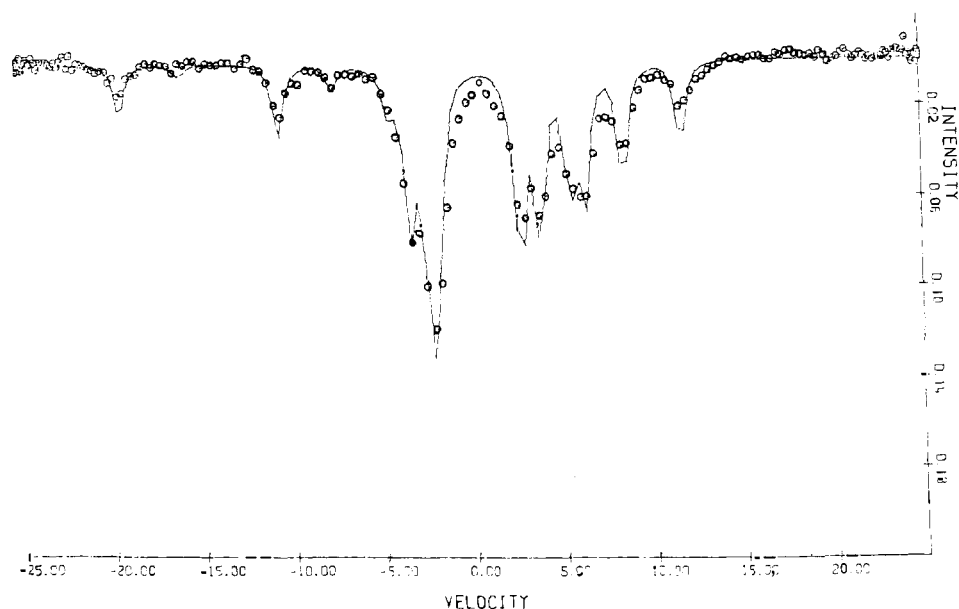


Figure 3. Iodine-129 Mössbauer spectrum of $\text{NiPcI}_{2.16}$. The solid line represents the optimized fit to the data points shown. Velocity is in mm/s.

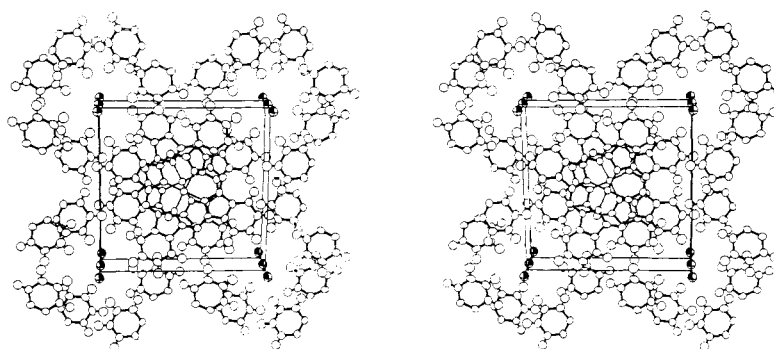


Figure 4. Stereoview of the crystal packing for $\text{NiPcI}_{1.0}$. Hydrogen atoms are shown as circles of arbitrary diameter.

diffraction data (vide infra). The optical absorption spectra of all materials with $x > 1$ are essentially identical.

NiPcI_x Iodine Mössbauer Spectroscopy. The iodine-129 Mössbauer spectrum of $\text{NiPcI}_{2.16}$ is shown in Figure 3. Computer analysis yielded the spectral parameters compiled in Table VI. The spectrum is typical of a symmetrical (D_{3h}) triiodide.^{11,25} There is no evidence of I^- ($\delta = -0.51$ mm/s, $e^2q^{129}Q = 0.00$ MHz)^{11,26} or I_2 ($\delta = +0.98$ mm/s, $e^2q^{129}Q = 1586$ MHz in frozen hexane solution)^{11,26} and it is estimated that these species are present to no greater than 3 and 5 mol %, respectively. Clearly the major, if not exclusive, iodine constituent is symmetrical I_3^- .

$\text{NiPcI}_{1.0}$ Single Crystal X-ray Investigation. The structure of $\text{NiPcI}_{1.0}$ consists of columnar stacks of NiPc well separated from linear chains of iodine, both running parallel to the z axis. The iodine chains are located in channels defined by the benzo groups of the nearby phthalocyanine ligands. A stereoview of the crystal packing is provided in Figure 4. The packing is considerably different from that in the unoxidized precursor, $\beta\text{-NiPc}$, in which the metallomacrocycle moieties are arrayed in slipped stacks. The iodine atoms lie on positions of 422 (D_4) symmetry, the NiPc molecule on $4/m$ (C_{4h}) sites. Owing to the crystallographically imposed $4/m$ symmetry, the NiPc molecule is rigorously constrained to be planar. Of the numerous metallophthalocyanine structures reported to date²⁷⁻³⁸ this compound is the first to have

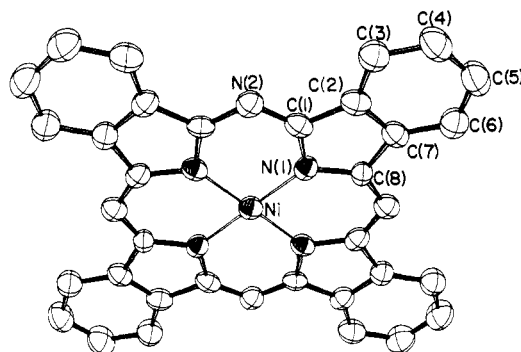


Figure 5. Perspective view of the NiPc macrocycle, hydrogen atoms omitted.

this crystallographic requirement. The Ni-N(1) distance of 1.887 (6) Å is similar to that observed in a number of four-coordinate phthalocyanine complexes of first-row metals.³⁹ Allowing for

(25) Potasek, M. J.; Debrunner, P. G.; Morrison, Jr., W. H.; Hendrickson, D. N. *J. Chem. Phys.* **1974**, *60*, 2203-2206.

(26) (a) Gibb, T. C. "Principles of Moessbauer Spectroscopy"; Chapman and Hall: London, 1976; Chapter 4.2. (b) Bancroft, G. M.; Platt, R. H. *Adv. Inorg. Chem. Radiochem.* **1972**, *15*, 59-258.

(27) Vogt, Jr., L. H.; Zalkin, A.; Templeton, D. H. *Inorg. Chem.* **1967**, *6*, 1725-1730.

(28) Brown, C. J. *J. Chem. Soc. A* **1968**, 2488-2493.

(29) Brown, C. J. *J. Chem. Soc. A* **1968**, 2494-2498.

(30) Hoskins, B. F.; Mason, S. A.; White, J. C. B. *Chem. Commun.* **1969**, 554-555.

(31) Ukei, K. *Acta Crystallogr., Sect. B* **1973**, *29*, 2290-2292.

(32) Fischer, M. S.; Templeton, D. H.; Zalkin, A.; Calvin, M. *J. Am. Chem. Soc.* **1971**, *93*, 2622-2628.

(33) Friedel, M. K.; Hoskins, B. F.; Martin, R. L.; Mason, S. A. *Chem. Commun.* **1970**, 400-401.

(34) Bennett, W. E.; Broberg, D. E.; Baenziger, N. C. *Inorg. Chem.* **1973**, *12*, 930-936.

(35) Gieren, A.; Hoppe, W. *Chem. Commun.* **1971**, 413-414.

(36) Rogers, D.; Osborn, R. S. *Chem. Commun.* **1971**, 840-841.

(37) Kirner, J. F.; Dow, W.; Scheidt, W. R. *Inorg. Chem.* **1976**, *15*, 1685-1690.

(38) Scheidt, W. R.; Dow, W. *J. Am. Chem. Soc.* **1977**, *99*, 1101-1104.

(39) For a short compilation of such distances see ref 37, Table XII.

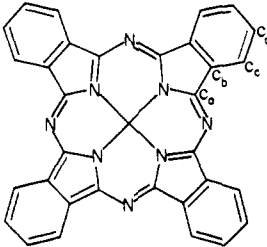
Table VII. Observed Distances and Angles in NiPcI

atoms	distance, Å	atoms	angle, deg
Ni-N(1)	1.887 (6)	N(1)-Ni-N(1')	90.00
N(1)-C(1)	1.370 (8)	C(1)-N(1)-C(8)	106.3 (6)
N(1)-C(8)	1.387 (8)	C(1)-N(2)-C(8')	119.2 (6)
N(2)-C(1)	1.313 (8)	N(2)-C(1)-N(1)	128.7 (7)
N(2)-C(8')	1.326 (9)	N(2)-C(1)-C(2)	119.8 (6)
C(1)-C(2)	1.451 (9)	N(1)-C(1)-C(2)	111.6 (6)
C(2)-C(3)	1.382 (10)	C(3)-C(2)-C(7)	121.1 (6)
C(2)-C(7)	1.392 (10)	C(3)-C(2)-C(1)	133.4 (7)
C(3)-C(4)	1.392 (10)	C(7)-C(2)-C(1)	105.5 (6)
C(4)-C(5)	1.394 (11)	C(2)-C(3)-C(4)	118.5 (7)
C(5)-C(6)	1.383 (10)	C(3)-C(4)-C(5)	119.8 (8)
C(6)-C(7)	1.392 (10)	C(6)-C(5)-C(4)	122.1 (8)
C(7)-C(8)	1.461 (9)	C(5)-C(6)-C(7)	117.4 (8)
		C(2)-C(7)-C(6)	121.0 (7)
		C(2)-C(7)-C(8)	106.9 (7)
		C(6)-C(7)-C(8)	132.1 (8)
		N(2)-C(8)-N(1)	128.4 (6)
		N(2)-C(8)-C(7)	121.9 (6)
		N(1)-C(8)-C(7)	109.6 (7)
		Ni-N(1)-C(1)	127.2 (5)
		Ni-N(1)-C(8)	126.4 (5)

the fact that the radius of the central hole of a phthalocyanine ring is about 0.11 Å smaller than that of a porphyrin molecule, this separation is also in agreement with the suggestion by Hoard⁴⁰ that radial strain is minimized in metalloporphyrins when the M-N separation is ~2.01 Å. A perspective view of the molecule, together with the labeling scheme, is given in Figure 5. Bond lengths and angles are compiled in Table VII. The bond lengths and angles reported here are similar to those of previously reported phthalocyanine complexes.^{27-38,41} For a quantitative comparison, the chemically distinct bonds have been averaged in accordance with D_{4h} symmetry and these values are given in Table VIII with similarly averaged data from a number of recent structural reports.⁴¹ NiPcI_{1.0} is in all respects similar to those previously reported, and evidently partial oxidation has had no measurable effect on the dimensions of the phthalocyanine ring. The average bond lengths and angles correspond well to the Kekule formula given above Table VIII, where the N_m-C_a , $N-C_a$, and C_a-C_b linkages are assigned π bond orders of $1/2$, $1/4$, and $1/4$, respectively. The average values for N_p-C_a and C_a-C_b of 1.376 (10) and 1.453 (3) Å are also in good agreement with the values of 1.379 (6) and 1.443 (5) Å observed for metalloporphyrins.⁴² As noted previously the $C_a-N_m-C_b$ angle is slightly contracted relative to the $C_a-C_m-C_b$ angle in the porphyrin analogues but the effect is not as large as originally thought. This contraction has been attributed to the steric requirements of the lone-pair electrons on atom N_m . All bond lengths in the fused benzene ring are found to be equivalent: their average value of 1.392 (6) Å compares well with the value for benzene. It is evident, however, that not all angles within the fused benzene ring are equivalent, the average $C_b-C_c-C_d$ angle being significantly compressed at 117.3 (2)° as compared with the others which are found to be equivalent at 121.4 (2)°. This effect has been noted previously,^{27,33} but is not peculiar to the phthalocyanine macrocycle. The same effect is observed frequently in hydrocarbon structures and has been attributed to strain resulting from fusion with a five-membered ring.⁴³

The crystal packing in NiPcI_{1.0} is similar to that reported for the partially oxidized metalloporphyrin systems Ni(dpg)₂I (dpg = diphenylglyoximate),^{5b} Ni(OMTBP)I (OMTBP = octamethyltetrabenzoporphyrinato),^{4a,d} Ni(tetrabenzoporphyrin)I,⁴⁴ and

Table VIII. Comparison of Bond Parameters in NiPcI with Those in MgPc, ZnPc, FePc, and MnPc



bond parameter ^{a,b}	NiPcI	mean ^c
Distances (Å)		
N_p-C_a	1.379 (12)	1.376 (10)
N_m-C_a	1.320 (9)	1.328 (7)
C_a-C_b	1.456 (7)	1.453 (3)
C_b-C_b	1.392 (10)	1.395 (4)
C_d-C_d	1.394 (11)	1.394 (2)
C_b-C_c	1.387 (7)	1.394 (2)
C_c-C_d	1.388 (6)	1.385 (7)
Angles (deg)		
$C_a-N_p-C_a$	106.3 (6)	108.1 (8)
$N_p-C_a-C_b$	110.6 (14)	109.3 (4)
$C_a-C_b-C_b$	106.2 (10)	106.7 (3)
$C_a-C_b-C_c$	132.8 (9)	132.2 (2)
$C_b-C_c-C_d$	118.0 (8)	117.3 (2)
$C_b-C_b-C_c$	121.05 (7)	121.3 (2)
$C_d-C_d-C_c$	121.0 (16)	121.6 (1)
$N_p-C_a-N_m$	128.6 (2)	127.7 (1)
$C_a-N_m-C_d$	119.2 (6)	123.2 (5)

^a N_p = pyrrole nitrogen; N_m = azamethine nitrogen. ^b Numbers in parentheses are deviations of a single observation if averaging was possible. ^c These are the average values from MgPc,³² ZnPc,³⁸ FePc,³⁷ and MnPc.³⁷

$M(\text{bqd})_2\text{I}_{0.5}^{1/2}\text{S}$ ($M = \text{Ni, Pd}$; $\text{bqd} = 1,2\text{-benzoquinonedioximate}$; $\text{S} = \text{aromatic solvent}$).^{3c,45} In the Ni(dpg)₂I, Ni(OMTBP)I, and NiPcI_{1.0} structures, a column of metal-ligand moieties is surrounded by four parallel tunnels containing polyiodide molecules (I_5^- in the former, I_3^- in the latter cases). In contrast, a $M(\text{bqd})_2$ column is surrounded by two tunnels containing polyiodide (I_3^-) and two containing solvent molecules.^{5c} Viewed normal to the z axis the present structure consists of separate layers of iodide atoms and sheets of nickel complex separated by $1/4c$; this is also the case for Ni(OMTBP)I and Ni(bqd)₂I_{0.5}^{1/2}S, but not for Ni(dpg)₂I. Successive phthalocyanine rings in the stack are staggered 39.5°, the closest intermolecular contacts in the stack being C(1)-C(1') and C(8)-C(8') at 3.252 (2) and 3.258 (2) Å, respectively. In the dimeric complex (MnPyPc)₂O,²⁷ the phthalocyanine rings are approximately parallel, separated by about 3.4 Å and staggered at 41°. In the phthalocyanine sandwich complexes of Sn³⁴ and U³⁵ the rings are much closer together (2.7-2.8 Å) and also staggered by about 40°. It was suggested that the yet unknown 45° staggered arrangement would result in unfavorable contacts between α -pyrrole carbon atoms in Sn-(Pc)₂.³⁴ In the present structure the 45° arrangement would not necessarily increase benzo-hydrogen atom contacts in the sheet, but it would decrease the C(1)-C(1') (and C(8)-C(8')) separations by 0.014 Å.

A most unusual feature of the present structure is the packing within the iodine chains. The observed I-I distance of 3.244 (2) Å is nearly 1.0 Å shorter than twice the van der Waals radius for I^- of 2.51 Å.⁴⁶ The thermal parameter along the chain direction is twice that perpendicular to the chain (Table III). We interpret these observations as indicating disorder of the iodine atoms and thus identify this as the cause of the diffuse scattering

(45) Endres, H.; Keller, H. J.; Moroni, W.; Weiss, J. *Acta Crystallogr., Sect. B* 1975, 31, 2357-2358.

(46) Pauling, L. "The Nature of the Chemical Bond", 3rd ed.; Cornell University Press: Ithaca, N.Y., 1960.

(40) Hoard, J. L.; Hamor, M. J.; Hamor, T. A.; Caughey, W. S. *J. Am. Chem. Soc.* 1965, 87, 2312-2319.

(41) For an extensive tabulation see: Day, V. M.; Marks, T. J.; Wachter, W. A. *J. Am. Chem. Soc.* 1975, 97, 4519-4527, Table VII.

(42) Hoard, J. L. In "Porphyrins and Metalloporphyrins", Smith, K. M., Ed.; American Elsevier: New York, 1975; pp 328-335.

(43) Christensen, A. T.; Thom, E. *Acta Crystallogr., Sect. B* 1971, 27, 581-586.

(44) Phillips, T. E.; Martinsen, J.; Pace, L.; Hoffman, B. M.; Ibers, J. A., manuscript in preparation.

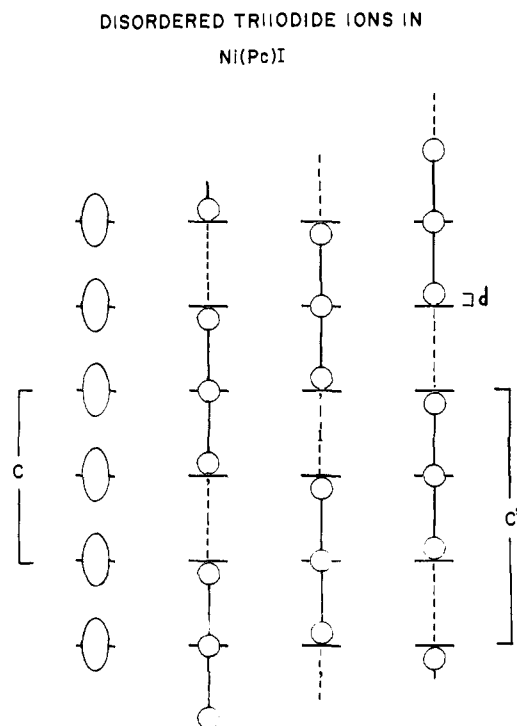


Figure 6. Disorder model for the iodine chains in NiPcI_{1.0}. Average positions are shown on the left; the three distinct supercells each containing three such sites are shown with the same scale on the right.

(see Experimental Section). The same conclusion was reached by Endres et al. for Ni(bqd)₂I_{0.5}.^{5c}

The observed planes of diffuse intensity normal to the *z* axis imply one-dimensional order along *z*, and the spacing of the diffuse lines, $c^* = 2/3c^*$, indicates that the repeat unit contains three Bragg sites. A reasonable model to account for this is the existence of ordered chains of I₃⁻ ions which are disordered with respect to their neighbors as shown in Figure 6. In each supercell two iodine atoms are displaced by an amount *d* from their average (Bragg) positions while one remains fixed, resulting in infinite chains of symmetric triiodide ions. Note that there are three distinct ways in which these chains can be ordered with respect to the arbitrary origin of the crystal. The intensity formula for this model⁴⁷ can be derived in a variety of ways; eq 2 is obtained as a special case of a more general formula $(|F_d(l)|^2 = \langle FF^* \rangle - | \langle F \rangle |^2)$ by Guinier, and is as follows:

$$|F_d(l)|^2 = (1/9)[(1 + 2 \cos [2\pi l(d - 1/3)])^2][9 - (1 + 2 \cos [2\pi l/3])^2] \quad (2)$$

where *l* refers to the supercell spacing $c' = 3/2c$. The general features of eq 2 are such that the left-hand bracketed quantity vanishes for *d* = 0 (i.e., no disorder), and the right-hand quantity for *l* = 3*n* (in agreement with experiment). It was the latter restriction which prevented the model in Figure 6 from being used for Ni(bqd)₂I_{0.5}, since there lines for *l* = 3*n* were observed. A least-squares fit of the diffuse intensities to eq 2 leads to a value of *d* of 0.0245 (2). This corresponds to an I-I distance within the triiodide ion of 3.00 Å and I---I nonbonded contacts of 3.72 Å. Observed and calculated structure amplitudes are given in Table IX; the final *R* index for the diffuse lines is 0.085. In view of the simplicity of the model, e.g., the explicit assumption of a symmetric I₃⁻ ion, the agreement is very satisfactory. It is doubtful that these limited data are amenable to analysis with a more complex model. The distances extracted from the diffuse intensity data are within the range 2.8–3.1 Å reported for triiodide ions,^{48,49}

Table IX. Observed and Calculated Structure Amplitudes for Diffuse Lines in NiPcI

<i>l</i>	<i>F</i> _o	<i>F</i> _c
1	19.4	14.4
2	25.3	23.0
4	43.7	46.0
5	33.3	31.7
7	55.7	53.9
8	20.4	21.8
10	42.3	44.0
11	4.5	8.1

R = 0.081

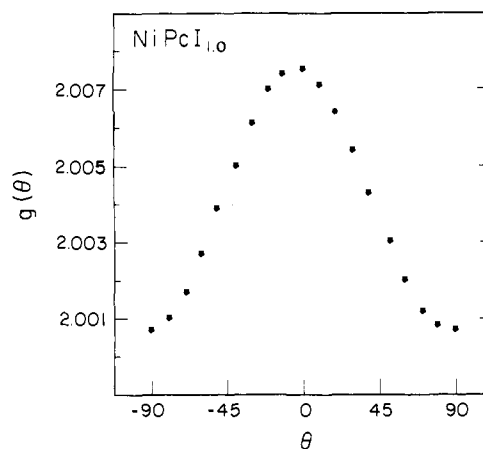


Figure 7. Angular dependence of the *g* value for the ESR signal of NiPcI_{1.0}. The orientation $\theta = 0$ is such that the principal crystal axis is parallel to *H*₀.

although bond distances >2.96 Å are ordinarily observed in asymmetric ions. The results support the existence of symmetrical I₃⁻ ions in NiPcI in complete agreement with the spectral data.

NiPcI_{1.0} Electron Spin Resonance *g* Values. NiPcI_{1.0} crystals show a single, moderately intense, rather narrow ESR signal whose *g* value and line width are angle dependent. The detailed study of the signal serves to identify the nature of the orbital which loses an electron upon partial oxidation of the NiPc. A combination of measurements of ESR and static susceptibility give evidence regarding the interaction within a partially oxidized NiPc stack.

The *g* tensor for NiPcI_{1.0} crystals is axially symmetric with the needle (molecular normal) *c* axis corresponding to the unique tensor axis. Figure 7 plots *g*(θ), the angle-dependent ambient temperature *g* value for a representative NiPcI_{1.0} crystal, where θ is the angle between the magnetic field *H*₀ and *c*. The *g* values can be fit to the equation

$$g(\theta) = [g_{\parallel}^2 \cos^2 \theta + g_{\perp}^2 \sin^2 \theta]^{1/2} \quad (3)$$

with $g_{\parallel} = 2.0075$ (2) and $g_{\perp} = 2.0007$ (2) for NiPcI_{1.0}. The observed angle dependence and the appreciable intensity of the signal unambiguously indicate that it represents the paramagnetic resonance of the hole species produced by partial oxidation and not an impurity.

Both g_{\parallel} and g_{\perp} are very close to the free-electron value of $g_e = 2.0023$. A metal-centered oxidation, however, would yield a hole species with the *g* value of [Ni^{III}Pc]⁺, far from g_e . The *g* values for [Ni^{III}Pc]⁺ have been found to be $g_{\perp} = 2.29$ and $g_{\parallel} = 2.11$.⁵⁰ The combination of nearly free-electron *g* values and narrow line widths is characteristic of the phthalocyanine π cation radical, [Ni^{II}Pc⁺], demonstrating that the oxidation is ligand centered. Since partial oxidation involves removal of electrons from the highest occupied π orbitals we may write with certainty the formula for the NiPcI_{1.0} as NiPc(I₃⁻)_{0.33} = [Ni^{II}Pc]^{0.33+} (I₃⁻)_{0.33}.

(47) Guinier, A. "X-ray Diffraction in Crystals, Imperfect Crystals and Amorphous Bodies"; W. H. Freeman: San Francisco, 1963; p 165.

(48) Popov, A. I. In "Halogen Chemistry"; Gutmann, V., Ed.; Academic Press: New York, 1967; Vol. 1, p 225.

(49) Runsink, J.; Swen-Walstra, S.; Migchelsen, T. *Acta Crystallogr., Sect. B* 1972, 28, 1331-1335.

(50) Bobrovskii, A. P.; Sidorov, A. N. *J. Struct. Chem. (Engl. Transl.)* 1976, 17, 50-54.

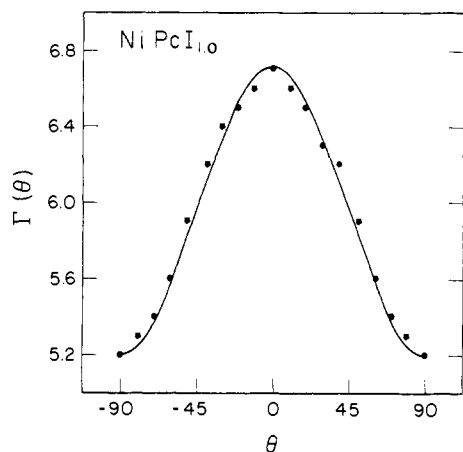
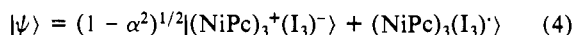


Figure 8. Angular dependence of the ESR line width at room temperature for NiPcI_{1.0}. Included (solid line) is the calculated dependence from the experimental data to eq 6 (see text).

A close inspection of the g tensor, nevertheless, shows it to be anomalous. For either a π -cation radical or a planar Ni^{III} species, we expect $g_{\parallel} \sim g_e$ and $g_{\perp} > g_e$. However, for NiPcI_{1.0}, we find $g_{\parallel} > g_{\perp} \approx g_e$. The observed deviation $g_{\parallel} > g_e$ is precisely of the form expected for the contribution of a fractional hole density on the iodine chain. If we represent the structure by the basic unit of (NiPc)₃⁺I₃⁻, the simplest way to account for spin density on iodine involves the inclusion of a small degree of back charge transfer. We schematically write a simple Mulliken charge transfer



wave function in which α^2 represents the degree of charge transferred from I₃⁻ back to the partially oxidized macrocycle. We show elsewhere that it is only possible to describe the results by assuming a ligand-centered oxidation of NiPc, and derive the formula^{4d}

$$g_{\parallel} \approx g_e + 2\alpha^2 \quad (5)$$

Employing the measured g_{\parallel} gives $\alpha^2 \approx 0.002$ as the degree of back charge transfer from an I₃⁻ ion to the macrocyclic stack.

NiPcI_{1.0} Electron Spin Resonance Line Width. The ESR line shape, although roughly Lorentzian in character, is asymmetric. The degree of asymmetry is typically expressed as the ratio of the amplitude of the larger amplitude lobe of the derivative line, A , to that of the smaller lobe, B . For NiPcI_{1.0} at room temperature, $A/B = 1.40 \pm 0.20$.^{51,52} This asymmetry is not due to the anomalous skin effect. First, the magnitude of the conductivity of NiPcI_{1.0} at room temperature, although large, should not cause A/B to differ appreciably from unity and A/B does not increase when σ_{\parallel} increases at low temperature. In addition, A/B is not a function of the angle (θ) between the needle c axis and the external field as seen in TSeF-TCNQ (TSeF = tetraselenafulvalene; TCNQ = tetracyanoquinodimethane).⁵³ Because the asymmetry is small and independent of both angle and temperature, further discussion of the line width will use the derivative peak-to-peak line width Γ .

Figure 8 shows the angle dependence of the peak-to-peak line width. The variation with angle (Figure 8) can be approximately fit to the expression¹⁴

$$\Gamma = \Gamma_0 + \Gamma_1(1 + \cos^2 \theta) \quad (6)$$

with $\Gamma_0 = 3.56$ and $\Gamma_1 = 1.76$ G. Γ_1 is relatively constant from crystal to crystal. Γ_0 ranges between 1.5 and 4.0 G and is larger with crystals of larger cross-sectional area. Thus there may be

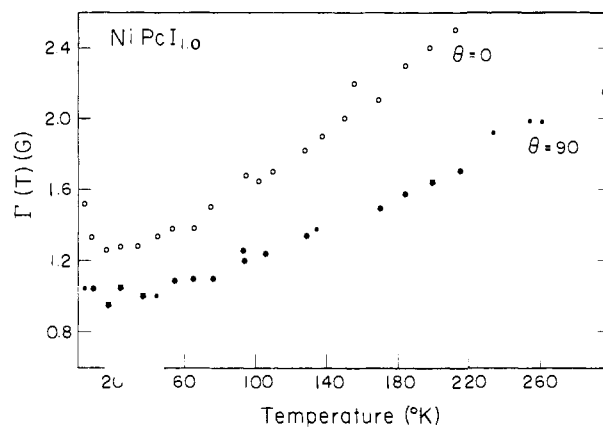


Figure 9. Temperature dependence of the ESR line width, $H_0 \parallel c$ (○) and $H_0 \perp c$ (●), for NiPcI_{1.0}.

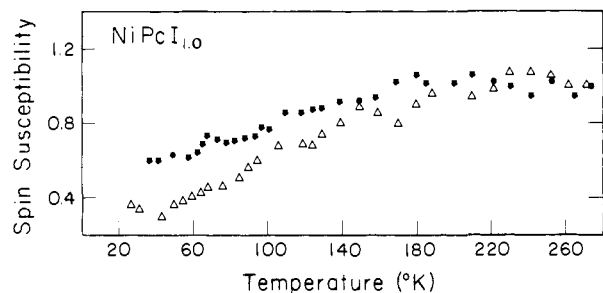


Figure 10. Temperature dependence of the intensity of the ESR signal of NiPcI_{1.0}, powder (●), single crystal (Δ), $H_0 \perp c$. All values are given relative to the intensity at 297 K.

a contribution from crystal mosaicity. This angle dependence is the same as that observed for Ni(OMTBP)I_{1.08}.^{4d} In this latter material the line width is found to be controlled by spin-lattice relaxation via polaron motion.⁵⁴ Even recognizing that the line width in NiPcI_{1.0} is exchange or motionally narrowed, we note that the small residual value is characteristic of π radicals, not of metal-centered moments.

The temperature dependence of Γ ($\theta = 0, 90^\circ$) for NiPcI_{1.0} is shown in Figure 9. The line width decreases slowly and approximately linearly with decreasing temperature down to 40–50 K, where there is a noticeable flattening of the curve. No sharp changes in the spin susceptibility, χ^s , are observed in the region of the conductivity transition (vide infra). Since the conductivity is metal-like in this region, the result suggests enhanced motional narrowing at lower temperature as carrier mobility is increasing. Alternatively, we note that in the Elliot line width mechanism, $\Gamma \propto (\Delta g)^2 \tau^{-1}$, where Δg is a measure of the g anisotropy and τ is the scattering time.⁵⁵ Since σ_{\parallel} and thus τ increase at lower temperatures, for constant Δg , Γ is expected to decrease as T decreases, as is observed. Note that the linear dependence, $\Gamma \propto T$, and quadratic dependence of the resistivity, $\rho_{\parallel} \propto T^2$ (vide infra), means that $\Gamma \propto \rho^{1/2}$.

NiPcI_{1.0} Magnetic Susceptibility. The room temperature ESR intensity of NiPcI_{1.0} was compared with that of DPPH and found to exhibit a spin susceptibility, χ^s , corresponding to 0.14 (3) spins per macrocycle. The temperature dependence of the scaled ESR integrated intensity, $I(T)/I(T_{297})$, for a powder of NiPcI_{1.0} is presented in Figure 10. The ESR intensity remains essentially constant from room temperature until approximately 180 K. Below approximately 180 K there is a gentle, roughly linear decrease until at 40 K, the lowest temperature examined, the intensity is about half that at room temperature. The data for a single crystal, Figure 10, suggest a slightly stronger falloff, but the ESR intensity from a single crystal is low, and in any case the difference in the measurements is not large.

(51) Feher, G.; Kip, A. F. *Phys. Rev.* **1955**, *98*, 337–348.

(52) Dyson, F. J. *Phys. Rev.* **1955**, *98*, 349–359.

(53) (a) Tomkiewicz, Y.; Engler, E. M.; Schultz, T. D. *Phys. Rev. Lett.* **1975**, *35*, 456–459. (b) Etemad, S.; Engler, E. M.; Schultz, T. D.; Penney, T.; Scott, B. A. *Phys. Rev. B* **1978**, *17*, 513–528.

(54) Phillips, T. E.; Hoffman, B. M.; Soos, Z. G. *Solid State Commun.* **1980**, *33*, 51–54.

(55) Elliott, R. J. *Phys. Rev.* **1954**, *96*, 266–279.

Table X. Conductivity Data for Polycrystalline Samples of Various NiPc_x Materials^a

compd	x	room temp conductivity, Ω ⁻¹ cm ⁻¹	activation energy for conductivity, eV ^b
NiPc _x	0	1 × 10 ⁻¹¹	1.6
	0.56	0.7	0.024
	0.58	2.2	
	1.0	0.7	0.036
	1.07	7.7	
	1.44	7.7	
	1.68	0.8	0.021
	3.81	0.6	

^a Pressed pellets studied by four-probe van der Pauw technique (see Experimental Section). ^b From least-squares fit to eq 13.

The measured static susceptibility of NiPc_{1.0} at room temperature is $\chi = -2.38 (25) \times 10^{-4}$ emu/mol. In order to obtain the diamagnetic correction, we have measured the susceptibility of NiPc, obtaining $\chi(\text{NiPc}) = -2.34 (25) \times 10^{-4}$ emu/mol. Adding to this the Pascal's constant susceptibility for $(I + I + \Gamma)/3$ ⁵⁶ as an approximation to the diamagnetism of $1/3$ of I_3^- , we arrive at $\chi^d = -3.49 (25) \times 10^{-4}$ emu/mol. The corrected paramagnetic susceptibility of NiPc_{1.0} is thus $\chi^p = +1.11 (35) \times 10^{-4}$ emu/mol, equivalent to 0.13 (4) electrons per site, in excellent agreement with the value of χ^s obtained by ESR spectroscopy. The static susceptibility, dominated by the diamagnetic terms, is essentially constant down to 4 K.⁵⁷

The weak temperature dependence of the spin susceptibility and metal-like conductivity (vide infra) of NiPc_{1.0} at high temperatures ($T > 180$ K) make it attractive to relate χ^s to the Pauli susceptibility of a degenerate electron gas. This permits an approximation of the intermolecular interaction within a stack of partially oxidized NiPc macrocycles in terms of t (the transfer integral), which is the one-electron matrix element for the intermolecular interaction. In a tight-binding band composed of the highest occupied molecular orbital on NiPc

$$\chi^s = 2\beta^2 D(\epsilon(k_f)) \quad (7)$$

where $\epsilon(k_f) = 2t \cos(k_f a)$ is the Fermi energy, k_f is the Fermi wave vector, and the one-dimensional density of states is given by

$$D(\epsilon(k)) = (N/2\pi)(4t^2 - \epsilon(k)^2)^{-1/2} \quad (8)$$

with N the number of molecules per cubic centimeter.^{2c} In NiPc_{1.0}, the highest band of occupied states is partially emptied by $b = 1/3$ of an electron/molecule, leading to

$$k_f = (2 - b)(\pi/2a) = 5\pi/6a \quad (9)$$

Thus the spin susceptibility for NiPc_{1.0} is

$$\chi^s = \beta^2 N / (2\pi t \sin(5\pi/6)) \quad (10)$$

When equated to the value of χ^p , this expression gives $t \sim 0.09$ eV and a bandwidth of $4t \sim 0.37$ eV. Although this model is an oversimplification, the value for t is of a reasonable magnitude for the overlapping ligand-centered π orbitals. Similar values for t have been found for other molecular metals.⁵⁸ A bandwidth of 0.20 eV is also found from thermoelectric power measurements and lends additional support for the application of one-dimensional tight-binding band theory to the properties of NiPc_{1.0}.^{59,60}

(56) Weisseberger, A.; Rossiter, B. W. "Physical Methods of Chemistry"; Wiley-Interscience: New York, 1969; Vol. 1, p 431.

(57) Unpublished results of A. Thompson, Exxon Research Laboratory, Linden, N.J., on samples of NiPc_{1.7}.

(58) Torrance, J. B.; Tomkiewicz, Y.; Silverman, B. D. *Phys. Rev. B* **1977**, *15*, 4738-4749.

(59) Unpublished results of R. L. Green, IBM Research Laboratories, San Jose, Calif. The measured thermoelectric power for NiPc_{1.0} was $s = +20$ $\mu\text{V}/\text{K}$.

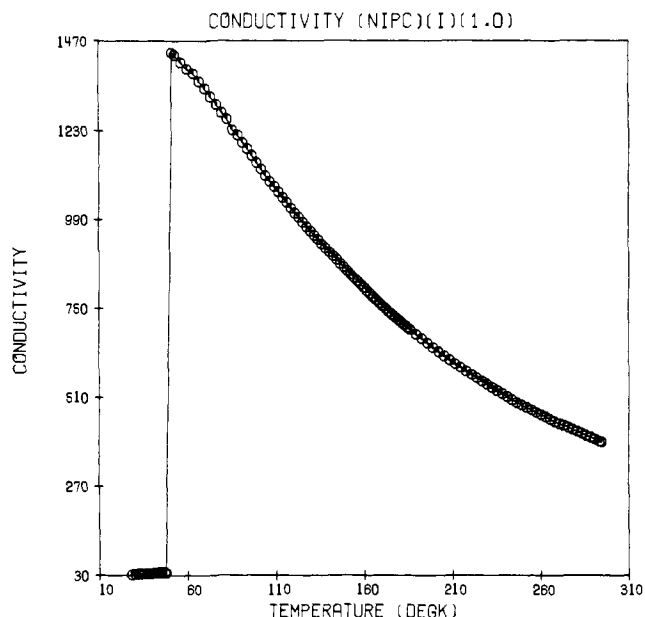


Figure 11. Temperature dependence of the conductivity for a NiPc_{1.0} crystal showing totally reversible behavior down to 25 K.

NiPc_x Electrical Conductivity. The electrical conductivity of NiPc_x materials for a range of x values is surveyed in Table X. These data are for compressed polycrystalline samples and as such suffer from interparticle contact resistance effects and from being averaged over all crystallographic orientations (more informative single crystal results will be discussed shortly). Nevertheless, the powder conductivity for a wide range of x are comparable with powder data for other "molecular metals", and experience with a variety of low-dimensional materials indicates that single-crystal conductivities along the molecular stacking direction should be greater by a factor of 10^2 – 10^3 . Variable-temperature studies of electrical conductivity were carried out for several powder samples and thermally activated charge transport was observed. Apparent activation parameters could be obtained by a least-squares fit to the equation

$$\sigma = \sigma_0 e^{-E_a/kT} \quad (11)$$

These parameters and standard deviations resulting from the fitting procedure are set out in Table X.

NiPc_{1.0} Single Crystal Conductivity. Single crystals of NiPc_{1.0} are exceedingly thin and electrical conductivity could only be measured along the needle axis. At room temperature, the conductivity range for 65 samples was 260–750 $\Omega^{-1} \text{cm}^{-1}$, with an average value of 550 $\Omega^{-1} \text{cm}^{-1}$. These values are comparable with stacking axis conductivities of "organic metals" such as TTF-TCNQ (tetrathiafulvalene-tetracyanoquinodimethane).^{2,62,63} However, because of the very large cross-sectional area of the phthalocyanine molecule, when comparing NiPc_{1.0} with other materials, it is instructive to consider the properties of the individual charge carriers. Within the framework of one-electron tight-binding band theory, the conductivity can be related to λ , the mean free path of a carrier along the stacking direction (the average distance between scattering events), and to a , the cross-sectional area per conducting stack, by the equation

$$\sigma_{\parallel} = 4e^2 \lambda / (ha) \quad (12)$$

where e is the electronic charge and h is Planck's constant.^{64,65}

(60) The temperature dependence of the spin susceptibility is also similar to that predicted theoretically for a one-dimensional antiferromagnetic Heisenberg chain⁶¹ with the appropriate band filling,⁵⁸ although the predicted χ^s is substantially higher than observed.

(61) DeJongh, L. J.; Miedema, H. R. *Adv. Phys.* **1974**, *23*, 1260.

(62) Devreese, J. T.; Evrard, V. E.; Van Doren, V. E., Eds. "Highly Conducting One-Dimensional Solids"; Plenum Press: New York, 1979.

(63) Torrance, J. B. *Acc. Chem. Res.* **1979**, *12*, 79-86.

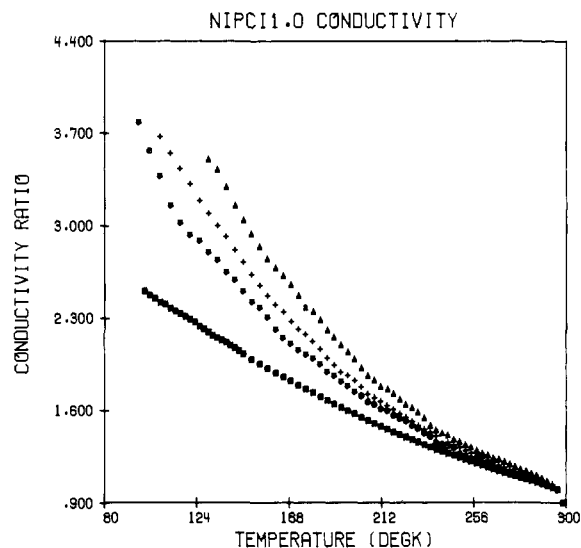


Figure 12. Temperature dependence of the conductivity ratio $\sigma_{\parallel}(T)/\sigma_{\parallel}(297 \text{ K})$ for four $\text{NiPcI}_{1.0}$ crystals at temperatures above their individual conductivity maxima.

For $\text{NiPcI}_{1.0}$ we find λ to be in the range 3.3–8.2 Å or 1.0–2.3 intermolecular spacings. This result can be compared with the values for other highly conducting stacked molecular systems of 2.1–2.8 spacings for $(\text{TTT})_2\text{I}_3$ (TTT = tetrathiatetracene),⁶⁶ 1–2 spacings for the related metallomacrocyclic Ni(tetrabenzoporphyrin)I,⁴⁴ 1.6–2.5 spacings for HMTSF–TCNQ (HMTSF = hexamethylenetetraselenafulvalene),⁶⁷ 0.4–0.6 spacing for TTF–TCNQ,⁶⁸ 0.6 spacing for $\text{K}_2\text{Pt}(\text{CN})_4\text{Br}_{0.3}\cdot 3\text{H}_2\text{O}$,^{2c} and 0.04 spacing for the polaronic conductor Ni(octamethyltetrabenzoporphyrin)I_{1.0}.^{4d,54}

Figure 11 shows a plot of the temperature dependence of $\text{NiPcI}_{1.0}$ conductivity along the *c* axis. As the temperature is decreased below ambient, all $\text{NiPcI}_{1.0}$ crystals exhibit a rise in conductivity to a maximum at temperature T_m , and then an abrupt decrease. T_m is found to vary from crystal to crystal, and, although typically about 100 K, T_m values between approximately 180 and 55 K were observed. Any crystal may be cycled repeatedly without hysteresis in σ_{\parallel} if *T* is maintained greater than T_m . Once cooled below T_m , however, most crystals never return to the initial room-temperature value of σ_{\parallel} upon warming. Upon recooling, the discontinuity occurs at a higher temperature T_m' , and at every temperature above T_m' the conductivity is less than had been measured on the initial cycle. Since contactless microwave measurements on $\text{NiPcI}_{1.0}$ show a reversible transition in σ_{\parallel} at the low end of our range of T_m values,⁶⁹ we conclude that in most instances the transition observed in the four-probe measurements is largely an artifact of stress on the crystal by the contact wires: the wires are typically of diameter comparable with a crystal.

Among the large number of $\text{NiPcI}_{1.0}$ crystals studied, and among those crystals showing the lowest T_m , one crystal (Figure 11) was seen to show a reversible “metal–semiconductor” transition for one cycle. The T_m value for this crystal is found to be ca. 52 K, which is equal within the experimental error of the temperature measurement to the T_m found in the microwave measurements. Because this crystal was mounted using 0.0005-in. diameter nickel wire, and was probably under much less stress than the majority

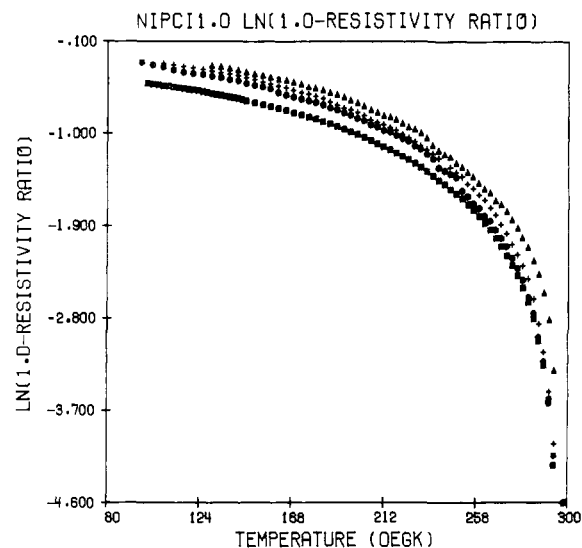


Figure 13. Plot of $\ln [1.0 - \rho(T)/\rho(297 \text{ K})]$ vs. temperature for the four $\text{NiPcI}_{1.0}$ crystals of Figure 12.

of $\text{NiPcI}_{1.0}$ crystals, with some confidence we use the reversibility of the transition at T_m as the criterion to assign the value of ca. 52 K as the true T_m for $\text{NiPcI}_{1.0}$. To provide further information on the nature of the 52 K transition, resonance Raman spectra of $\text{NiPcI}_{1.0}$ crystals were recorded down to 8 K. There was no change in the polyiodide scattering pattern which would indicate a change in the degree of charge transfer, i.e., appearance of an I_5^- or I_2 transition.

The analysis of the dependence of the $\text{NiPcI}_{1.0}$ conductivity in the region above T_m is not complicated by artifacts. All crystals cycled in the region T_m to 300 K show completely reversible behavior over three cycles, the maximum number performed. Thus for all crystals the data above T_m are taken as valid. Individual crystals show different $\sigma_{\parallel}(T_1)$ ($T_1 = 295 \text{ K}$) and plots of $\sigma_{\parallel}(T)/\sigma_{\parallel}(T_1)$ are not overlapping. Figure 12 illustrates this behavior for four $\text{NiPcI}_{1.0}$ crystals. However, the temperature dependence of all crystals studied obeys the empirical relationship⁷⁰

$$\rho(T)/\rho(T_1) = a + b(T/T_1)^{\nu} \quad (13)$$

where *a* and *b* are constants, with a least-squares fit of the data yielding the result $\nu = 1.9 \pm 0.2$. The value of ν is different from unity found for simple metals and is reminiscent of that found for several other molecular metals, 2.0–2.4.⁷¹ Crystals with the highest T_m give the poorest statistical fit to eq 13, probably because the data are obtained over a narrow range of temperature. In such cases the value of ν is not well determined and appears to vary from the value of 1.9 ± 0.2 exhibited by the majority of crystals. A similar apparent dependence of ν on the temperature range of the data has been noted elsewhere.^{70b}

From plots of $\sigma(T)/\sigma(T_1)$ vs. temperature it is not obvious that a single conductivity mechanism applies to all crystals of a given material. The four $\text{NiPcI}_{1.0}$ data sets in Figure 12 are a good example. As an alternative mode of presenting the conductivity, a plot of the quantity $\ln [1 - [\rho(T)/\rho(T_1)]]$ vs. temperature may be employed.⁷² As shown for the four representative $\text{NiPcI}_{1.0}$ crystals in Figure 12, this method yields a superimposable family of curves. The curves plotted in Figure 13 have not been overlapped in order that the behavior of each crystal may be easily observed. However, it is obvious that the lower three curves in Figure 13 would fully overlap the top curve. This result provides assurance of the reliability of the conductivity measurements and

(64) Berlinsky, A. J. *Contemp. Phys.*, **1976**, *17*, 331–354.

(65) Mott, N. F.; Davis, E. A. “Electronic Processes in Noncrystalline Materials”; Clarendon Press: Oxford, 1971.

(66) Issett, L. C.; Perez-Albuern, E. A. *Solid State Commun.* **1977**, *21*, 433–435.

(67) (a) Bloch, A. N.; Cowan, D. O.; Bechgaard, K.; Pyle, R. E.; Banks, R. H.; Poehler, T. O. *Phys. Rev. Lett.* **1975**, *34*, 1561–1564. (b) Greene, R. L.; Mayerle, J. J.; Schumaker, R.; Castro, G.; Chaikin, P. M.; Etemad, S.; La Placa, S. J. *Solid State Commun.* **1976**, *20*, 943–946.

(68) Etemad, S.; Engler, E. M.; Schultz, T. D.; Penney, T.; Scott, B. A. *Phys. Rev. B* **1978**, *17*, 513–528.

(69) Poehler, T., private communication.

(70) (a) Seiden, P. E.; Cabib, D. *Phys. Rev. B* **1976**, *13*, 1846–1849. (b) Chiang, C. K.; Cohen, M. H.; Newman, P. R.; Heeger, A. J. *Ibid.* **1977**, *16*, 5163–5172.

(71) Andre, J. J.; Bieber, A.; Gautier, F. *Ann. Phys. (Paris)* **1976**, *1*, 145–256.

(72) Groff, R. P.; Suna, A.; Merrifield, R. E. *Phys. Rev. Lett.* **1974**, *33*, 418–421.

of a well-defined scattering mechanism.

On the Nature of NiPcI_x Stoichiometries Where $x \neq 1$. As noted earlier, powdered samples of NiPcI_x can be prepared for a wide range of x . The resonance Raman and iodine Mössbauer results indicate that iodine is present predominantly if not exclusively as I₃⁻ up to $x \sim 3.0$. For $x \lesssim 1.0$, there is some evidence from the optical spectra that unoxidized NiPc may be present. However, from such results it is not clear whether starting bulk NiPc or discrete NiPc molecules (or groups of molecules) integrated into a NiPcI_x lattice are being observed. Indeed, the spectral data provide no information on whether a single phase with a continuously varying iodine content or phases of discrete stoichiometries (or ranges of stoichiometries) might be present. This problem was investigated by X-ray powder diffractometry on NiPcI_x samples where $x = 0, 0.55, 1.0, 1.1, 2.64,$ and 4.01 . Although the data were only evaluated in a semiquantitative fashion, the following conclusions could be reached. First, for $x < 1.0$, quantities of bulk, unoxidized NiPc were clearly present. The only other phase which could be detected was the $x = 1.0$ material. The presence of unoxidized NiPc is in accord with the optical spectra. Second, the materials with $x > 1$ contain no detectable NiPc. However in addition to varying amounts of the $x = 1.0$ material, they exhibit an additional phase with a new crystal structure, distinctly different from the $x = 1.0$ phase. No attempt was made to index this cell. Iodine oxidation of the related macrocycle Ni(OMTBP) has so far produced crystals with two stoichiometries, $x \approx 1$ and $x \approx 3$.^{4a,d} The present powder diffraction results for NiPcI_x suggest that there also may be only two phases with $x < 3$, one at $x = 1$, the other at $x \approx 3$.

Conclusions

Partial oxidation of metallophthalocyanines with iodine has provided an extensive new class of molecular conductors. As

illustrated in the present case with nickel phthalocyanine, the properties of the resulting solid-state array of π -cation radicals include electrical conductivity which is comparable with that of the best known stacked molecular conductors. A particularly intriguing feature of NiPcI_{1.0} charge transport is a transition from metallic to semiconducting behavior which apparently is not reflected in the magnetic properties of the carriers. It is tempting to speculate that this behavior reflects a change in carrier mobility brought about by some subtle structural rearrangement.

In a broader perspective, the iodinated metallophthalocyanines, such as those reported here, represent the first entry into a widening area of conductive materials based upon the ligand π systems of mixed-valent metallomacrocylic arrays. Clearly the insights gleaned and the methodology developed will lead to an ever-deepening understanding of those molecular characteristics which facilitate charge conduction and which optimize materials performance.

Acknowledgments. This research was generously supported by the NSF-MRL program through the Materials Research Center of Northwestern University (Grant DMR76-80847A01), by the NSF (Grant DMR77-26409 to B.M.H. and Grant CHE76-10335 to J.A.I.), and by the Office of Naval Research (to T.J.M.). We thank Professor J. B. Cohen for assistance with the diffuse scattering measurements and Mr. J. Martinsen for assistance in the static susceptibility measurements. We thank Dr. Stanley L. Ruby of the Physics Division of Argonne National Laboratory for recording the iodine Mössbauer spectrum of NiPcI_{2.16}.

Supplementary Material Available: The root-mean-square amplitudes of vibration (Table IV) and a listing of structure amplitudes (4 pages). Ordering information is given on any current masthead page.

Mechanism of Thermal Decomposition of Dineopentylbis(triethylphosphine)platinum(II): Formation of Bis(triethylphosphine)-3,3-dimethylplatinacyclobutane¹

Paul Foley, Robert DiCosimo, and George M. Whitesides*

Contribution from the Department of Chemistry, Massachusetts Institute of Technology, Cambridge, Massachusetts 02139. Received February 19, 1980

Abstract: The thermal decomposition of dineopentylbis(triethylphosphine)platinum(II) (**1**) in cyclohexane solution at 157 °C yields bis(triethylphosphine)-3,3-dimethylplatinacyclobutane (**4**) by a reaction which involves dissociation of 1 equiv of triethylphosphine, intramolecular oxidative addition of the C-H bond of a neopentyl methyl group to platinum (**3**), and reductive elimination of neopentane. Carbon-carbon bond formation resulting in production of dineopentyl is a detectable side-reaction. The overall reaction has Arrhenius activation parameters: $E_a \approx 49$ kcal mol⁻¹, $\log A \approx 20$. The activation energy for phosphine dissociation is 27-35 kcal mol⁻¹. Transfer of a hydrogen atom from the triethylphosphine group to a neopentyl moiety occurs at a rate approximately 3% that of transfer of hydrogen from the methyl of one neopentyl group to the methylene of the other. Any processes which abstract α -methylene hydrogens from the neopentyl group occur at less than 1% the rate of processes which abstract hydrogens from the neopentyl methyl groups. Substitution of deuterium for hydrogen in either the neopentyl methyl groups or the triethylphosphine groups slows the decomposition reactions ($k_H/k_D \approx 3.0$). The mechanism proposed for generation of **4** is based in part on deuterium-labeling experiments: comparison of results by using different labeling patterns for **1** demonstrates the special utility of "inverted" experiments in which *hydrogen* transfer from a specific site is examined in a system which is otherwise perdeuterated. The driving force for the conversion of **1** to **4** is not obvious: it may be relief of steric strain in **1**, changes in electronic energy due to reorganization of ligands around platinum, or changes in entropy.

Introduction

The cleavage of unactivated aliphatic C-H bonds by reaction with transition metals occurs in a number of useful heterogeneous catalytic processes; reforming,² dehydrogenation,³ and probably

platinum-catalyzed oxidation⁴ provide examples. Current efforts to develop *homogeneous* catalysts for C-H bond activation are justified on the basis that such catalysts might functionalize hydrocarbons selectively and that they might be amenable to detailed

(1) Supported by the National Science Foundation, Grants MPS 74-20956 and 7711282 CHE.

(2) Sinfelt, J. H. *Prog. Solid State Chem.* **1975**, *10*, 56-69; *Science (Washington, D.C.)* **1977**, *195*, 641-646.

(3) Clarke, J. K. S.; Rooney, J. J. *Adv. Catal.* **1976**, *25*, 125-183. Biloen, P.; Dautenberg, F. H.; Sachtler, W. M. H. *J. Catal.* **1977**, *50*, 77-86.

(4) Rylander, P. N. "Organic Synthesis with Noble Metal Catalysts"; Academic Press: New York, 1973; pp 99 ff. Dirks, J. M. H.; van der Baan, H. S.; van der Broek, J. M. A. *J. Carbohydr. Res.* **1977**, *59*, 63-72.